



Functional NiTi grids for *in situ* straining in the TEM



U. Schürmann^{a,1}, C. Chluba^{b,1}, N. Wolff^a, D. Smazna^c, R. Lima de Miranda^e, P. Junker^d,
R. Adelung^c, E. Quandt^b, L. Kienle^{a,*}

^a Institute for Materials Science, Synthesis and Real Structure, Christian Albrechts University, Kaiserstraße 2, Kiel D-24143, Germany

^b Institute for Materials Science, Inorganic Functional Materials, Christian Albrechts University, Kaiserstraße 2, Kiel D-24143, Germany

^c Institute for Materials Science, Functional Nanomaterials, Christian Albrechts University, Kaiserstraße 2, Kiel D-24143, Germany

^d Institute of Mechanics, University of Wuppertal, Gaußstraße 20, Wuppertal D-42119, Germany

^e Acquandas GmbH, Kaiserstraße 2, Kiel D-24143, Germany

ARTICLE INFO

Article history:

Received 6 October 2016

Revised 19 May 2017

Accepted 1 June 2017

Available online 9 June 2017

Keywords:

In situ straining

Transmission electron microscopy

Shape memory alloys

ZnO

Finite element simulations

ABSTRACT

In situ measurements are a pivotal extension of conventional transmission electron microscopy (TEM). By means of the shape memory alloy NiTi thin film Functional Grids were produced for *in situ* straining as alternative or at least complement of expensive commercial holders. Due to the martensite-austenite transition temperature straining effects can be observed by use of customary heating holders in the range of 50 to 100 °C. The grids can be produced in diversified designs to fit for different strain situations. Micro tensile tests were performed and compared with finite element simulations to estimate the applied forces on the sample and to predict the functionality of different grid designs. As a first example of this Functional Grid technology, we demonstrate the impact of applying a strain to a network of ZnO tetrapods.

© 2017 Elsevier B.V. All rights reserved.

1. Introduction

In the last years, the increasing necessity for *in situ* observations in analytical methods becomes apparent. In the field of transmission electron microscopy a wide range of parameters have been altered inside the instrument. Next to the examination of temperature dependent properties where *in situ* heating holders are widely-used also electrical biasing, electrochemical reactions, electron beam irradiation as well as mechanical and tensile testing were examined [1–6]. Even for novel and sophisticated setups using TEM-compatible MEMS devices one drawback of all these methods is often the need for dedicated and expensive devices and holders [7,8].

In this work we present a new approach for *in situ* straining of samples by using a Functional TEM Grid composed of shape memory alloy (SMA) Nickel-Titanium thin films which can be utilized inside a common TEM heating holder at moderate temperatures. Morphological changes, phase transformations, straining effects, defect propagation and other mechanical induced phenomena are intended to be observed with this technique.

The shape memory effect of NiTi alloys depends on the martensitic phase transformation between the cubic high temperature

phase austenite and the tetragonal low temperature phase martensite. This well-known effect is described in detail in the literature [9–11]. Cooling from the austenite phase results in a twinned martensite, which keeps the macroscopic shape of the austenite phase. The twinned martensite consists of three twin variants with different *c*-axis orientation. Deformation occurs via detwinning of this martensite leading to a macroscopic shape change with up to 8% strain. Application of moderate heating initiates back transformation into the austenite phase and as a result the material recovers its original shape.

These austenitic transformation temperatures strongly depend on the alloys composition with marginal variations and can be tailored precisely by variation of fractions of an atomic percent. The composition of the alloy used in this study was chosen to provide an austenite start temperature well below 100 °C to avoid side effects on the sample during straining like undesired phase transitions.

To achieve an effect on the material to be tested, a sufficiently high force has to be applied on the sample. This force can be determined directly by tensile test measurements or estimated indirectly by finite elements methods (FEM). Both methods were combined to draw conclusions about the utility of the Functional Grids. Furthermore the feasibility of FEM on the presented design shows the possibility to predict the suitability of other and more complex designs in order to conduct variable kinds of deformation experiments in TEM.

* Corresponding author.

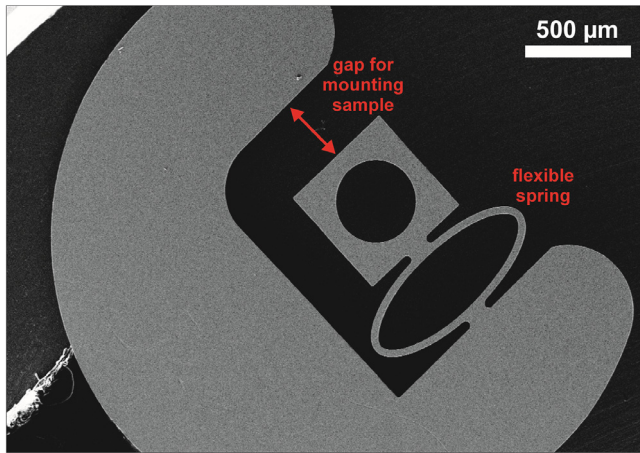
E-mail address: lk@tf.uni-kiel.de (L. Kienle).

¹ U. Schürmann and C. Chluba contributed equally to this work.

Table 1

Used model parameters. Details on the model and the respective meaning can be found in [16,17].

Transformation strain η	0.051 [-]	Poisson's ratio for transformation ν_T	0.45 [-]
Elasticity module austenite E_A	60 [GPa]	Poisson's ratio for austenite ν_A	0.35 [-]
Elasticity module martensite E_M	40 [GPa]	Poisson's ratio for austenite ν_M	0.35 [-]
Enthalpy constant a	5.5 [MPa]	Entropy constant b	0.23 [MPa/K]
Dissipation parameter r	4.1 [MPa/s]		

**Fig. 1.** SEM image of a NiTi grid in relaxed martensitic state at ambient temperature.

We demonstrate the effectiveness of the Functional Grid on a ZnO tetrapod network produced within the recently introduced flame transport synthesis (FTS) [12,13].

2. Experimental

The Functional Grid device fabrication was performed by clean-room technology following a flow chart described in detail elsewhere [14,15]. The relevant steps to obtain freestanding structured NiTi films comprise sputter deposition onto pre-structured sacrificial layers followed by chemical wet-etching. Two different setups were investigated: the as-obtained amorphous films possess a composition of $Ti_{51}Ni_{49}$ and thickness of $\sim 50\mu m$ and $\sim 40\mu m$, respectively. Crystallization and adjustment of the transformation temperatures is conducted by a sequential heat treatment at $650\text{ }^\circ\text{C}$ for 10 min using rapid thermal annealing. Diversified designs can be realized with respect to individual application. *In situ* straining experiments were carried out in a TEM Tecnai F30 STwin microscope (300 kV, field emission gun (FEG) cathode, spherical aberration coefficient $C_s = 1.2\text{ mm}$) using a double-tilt heating holder (Gatan). A Zeiss Gemini Ultra55Plus was applied for scanning electron microscopy (SEM).

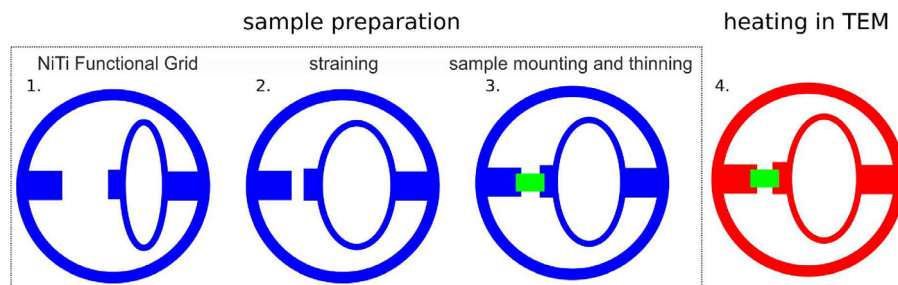
To determine the force displacement curve of the Functional Grid during application a combination of micro tensile tests and simulation was utilized. Tensile tests have been performed using a self-built micro tensile test setup consisting of an actuator (PI M-229.26S) and a load cell (ME KD24s 10 N). During testing the grid deformation was observed using an optical microscope. For the mechanical tests grids with two different strut widths of $50\mu m$ and $40\mu m$ are used.

Along with the experimental investigations, numerical simulations of the $50\mu m$ grid based on a variational material model for shape memory alloys were performed. The model solely relies on energetic material parameters, i.e. for the dissipated energy due to phase transformations. This allows for one single model calibration. It has been shown in [16] and [17] that the model can be calibrated using either tensile tests at two different temperatures or one single digital scattering calorimetry (DSC) measurement. This unique property of the model ensures a huge reliability of the numerical results. The model was implemented into the finite element code FEAP and the parameters according to Table 1 were used.

The numerical simulations provide assistance to understand the evolving phase transitions and indicate the parts of the specimen under maximum stress/load. Furthermore, an investigation of the interplay between geometry and mechanical / thermal loading can be employed.

For the visualization of a straining experiment a small amount of ZnO network (macroscopically appearing as “wool”) was fixed to the pre-strained Functional Grid across the gap by using UV hardened, commercially available glue. The ZnO wool consists of a variety of micron-sized crystal morphologies including wires, tetrapods and flakes, which are interconnected and forming in such a manner a 3D network.

The ZnO 3D network was prepared by a modified flame transport synthesis (FTS). During the FTS that is introduced in our previous publications [12,13] the Zn particles get oxidized in normal atmosphere of the furnace and a polyvinyl butyral (PVB) component is burned creating a defined oxygen atmosphere. When the temperature has reached $900\text{ }^\circ\text{C}$ the vaporized Zn oxidizes and is deposited on the walls of the ceramic crucible where the precursors are placed initially. In a new modified approach no polymer precursor is used, but the small amount of Zn (covering less than

**Fig. 2.** Schematic of the Functional Grid concept: sample preparation at room temperature and TEM analysis by using a heating holder. 1. Sketch of the Functional Grid in the relaxed martensitic state, 2. Pre-straining of the grid introduces deformation and local detwinning of the martensite. 3. Sample (green) mounting 4. Afterwards, the grid is transferred to a TEM heating holder. During analysis the temperature of the grid is increased and force acting on the specimen is built up during the martensite-to-austenite transformation process recovering its original shape as depicted in 1. (For interpretation of the references to colour in this figure legend, the reader is referred to the web version of this article.)

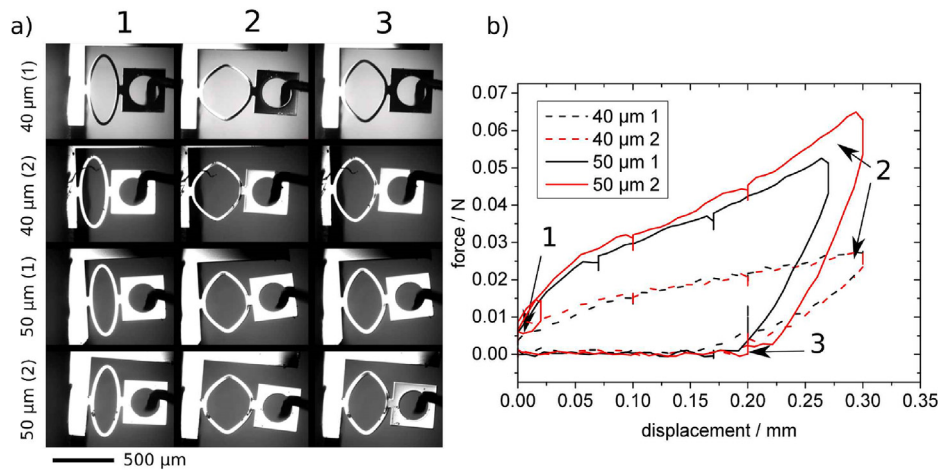


Fig. 3. Pre-straining experiments of four grids with 40 μm and 50 μm spring width, respectively. a) shows the deformation at three stages 1 (undeformed), 2 (stressed), and 3 (unloaded/deformed) denoted in the corresponding stress strain curve b). The drop-off in the force at several reading points are caused by the interruption of the measurement due to image capturing.

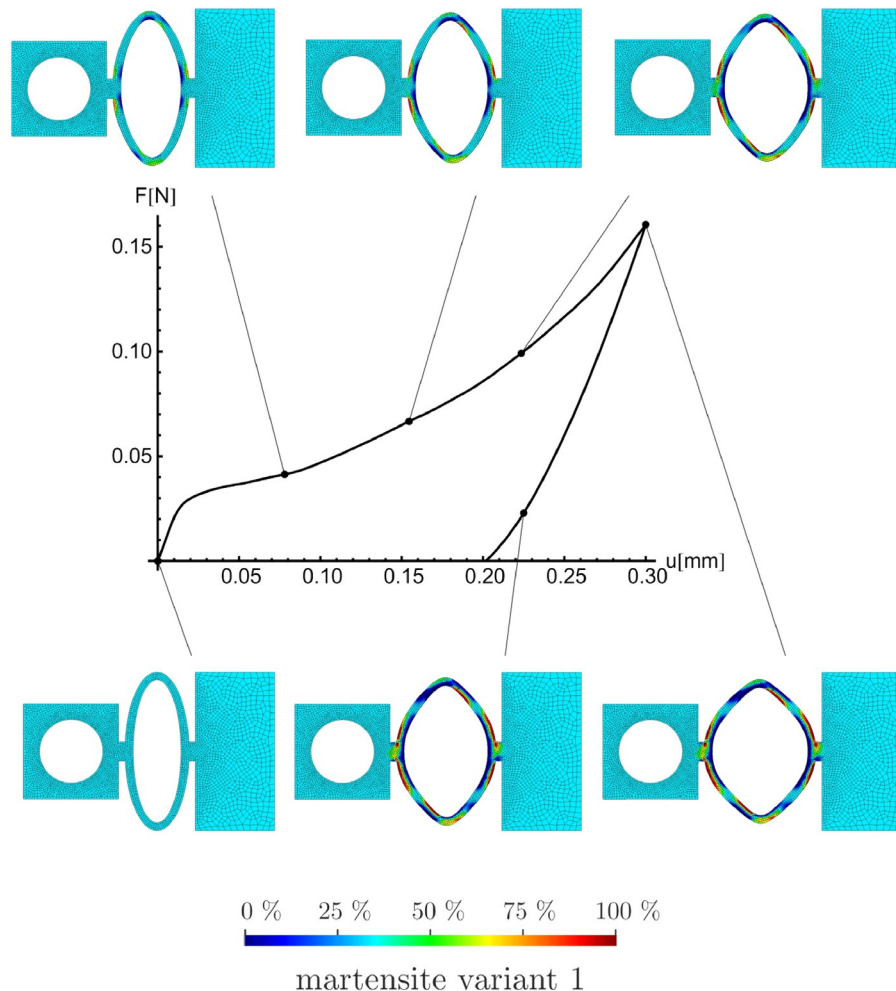


Fig. 4. Calculated stress strain curve by FEM and distribution of one martensite variant over the Functional Grid during six states of the pre-straining process (exact description see text).

10% of the ceramic crucible) is placed into the furnace preheated to 900 °C and containing of 90% nitrogen atmosphere. When the Zn is converted to vapor after 7 minutes, nitrogen flow is changed to pressured air and the reaction of Zn oxidation takes place creating a 3D interconnected network of ZnO structures.

3. Results

The functionality of the thin film Functional Grids relies on a compact semi-opened ring ending up in spring-like flexible parts where the grid can be pre-strained upon introducing the de-twinned martensitic phase. An SEM image showing one of the

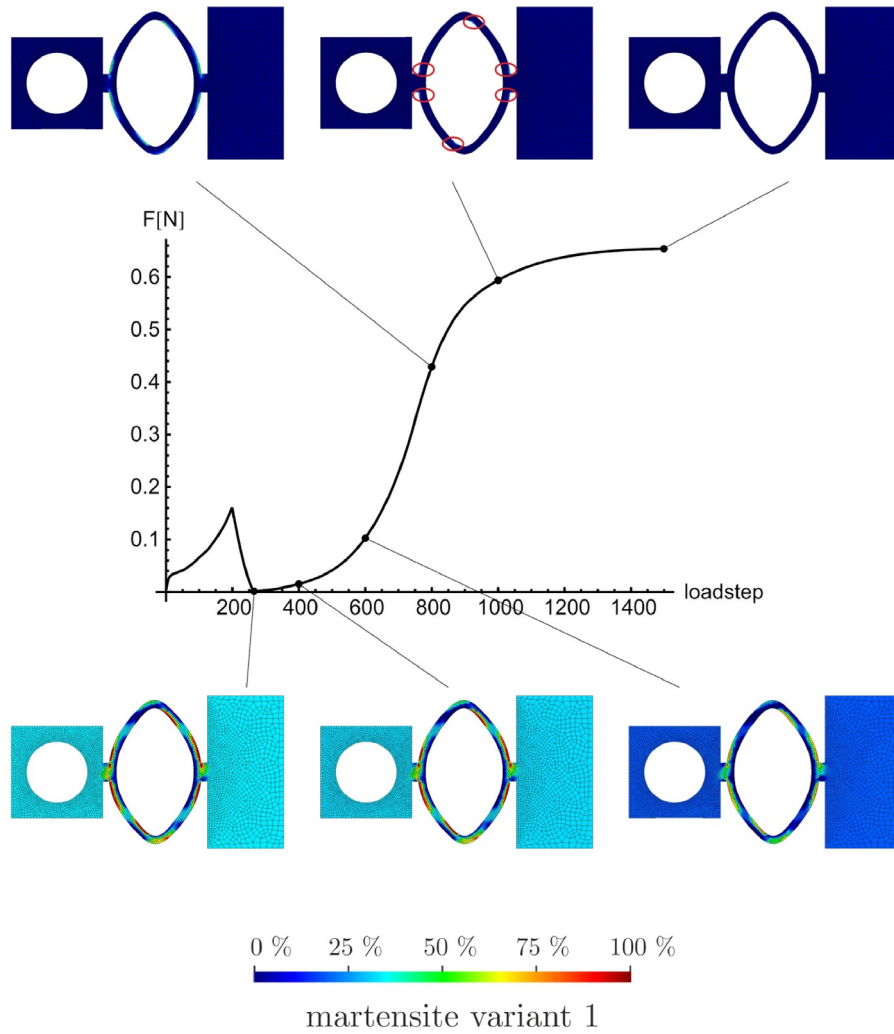


Fig. 5. Force/displacement curve of the specimen over the loadsteps during pre-straining (up to load step 265) and subsequent heating. The increasing amount of blue areas is an indication of the propagating austenitic phase. The red circles emphasize very small martensitic zones, where remarkable higher temperature is needed for the back transformation, responsible for the decreasing slope of the curve. (For interpretation of the references to colour in this figure legend, the reader is referred to the web version of this article.)

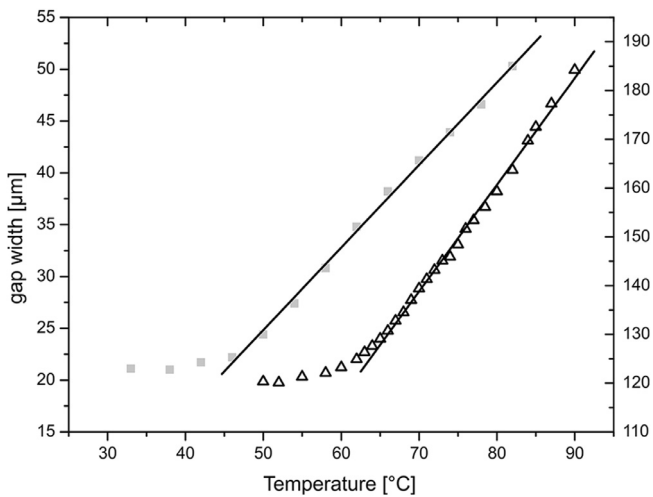


Fig. 6. Temperature dependence of the gap width of two Functional Grids with different designs and starting width after pre-straining. Squares representing design with starting width of 20 μm (left axis), triangles representing design with starting width of 120 μm (right axis). Linear fits are given starting at the austenite starting temperature.

tested designs is depicted in Fig. 1. The active region is assumed to be located inside edges of the filigree arms of the spring. At this flexible component pre-straining is necessary to minimize the gap where the actual sample should be mounted. During heat treatment above the austenite starting temperature, e.g. inside TEM, the spring arms re-transform into the austenitic phase retaining its original shape, thereby applying strain onto a mounted sample. The process sequence is depicted schematically in Fig. 2 on the basis of a principle Functional Grid design.

3.1. Micro tensile testing

Micro tensile testing experiments were performed to determine the forces at the pre-straining and to measure the forces applied during the *in situ* TEM experiments. Two designs with a structure thickness of 40 μm and 50 μm were tested, in which two grids of each design were used for reproducibility. The deformation states (1. undeformed, 2. stressed and 3. unloaded/deformed) as well as the stress-displacement curves are shown in Fig. 3. The required force for pre-straining is twice the value of the 50 μm compared to the 40 μm structure size but the remaining deformation after unloading is with $\sim 200 \mu\text{m}$ comparable for both. Reproducibility derivations of the deformation micrographs and the stress-

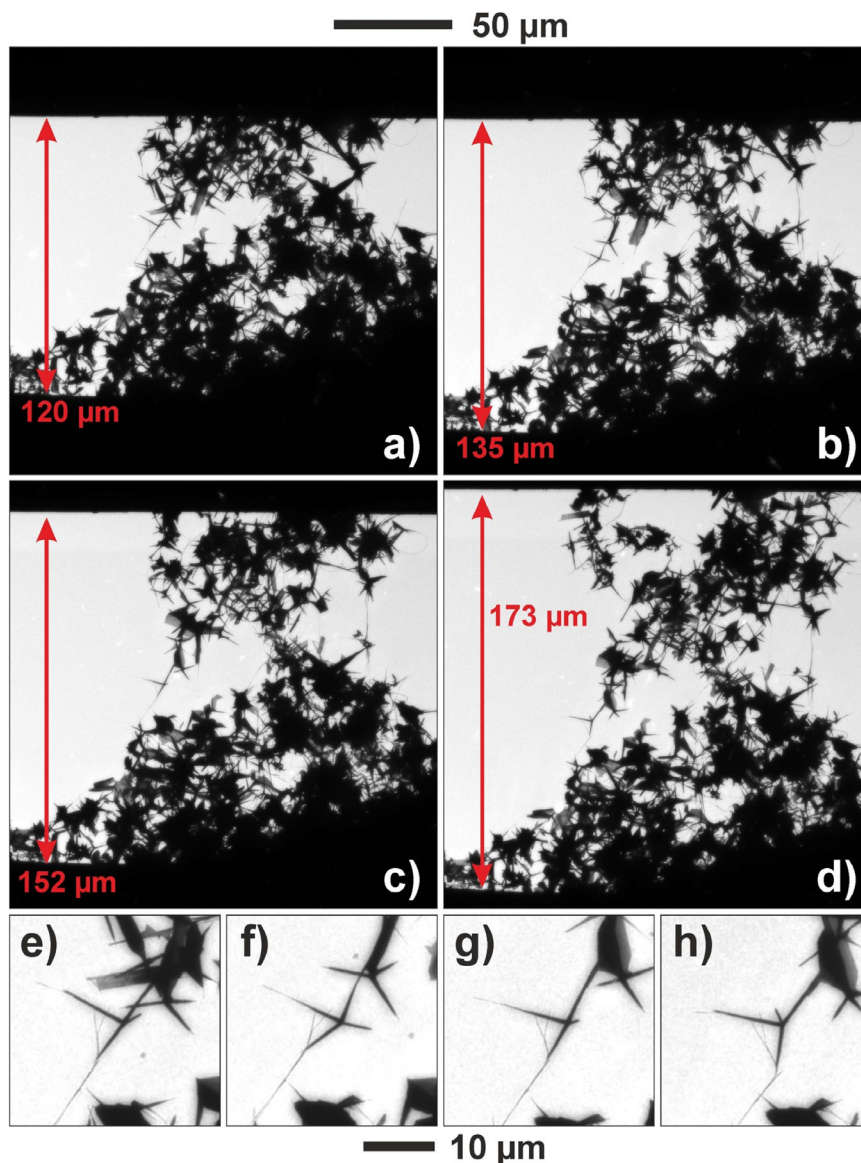


Fig. 7. First *in situ* straining experiments via Functional Grids. TEM Images at low magnification showing the gap of a grid loaded with a ZnO network at different temperatures: a) 50 °C, b) 68 °C, c) 76 °C and d) 85 °C. An enlargement of a detail showing a rotating tetrapod at the same temperatures is given in e–h).

displacement results are considered to be caused by the sample mounting and not by the structure itself. This problem is likely to be solved by using more advanced handling and mounting techniques which can be easily implemented by additional structuring.

3.2. Finite elements simulation

Finite elements methods were applied for more exact determination of the transition process of the Functional Grids. Questions to be addressed are the magnitude of the martensitic-austenitic transformation zone, the prediction which design may fulfil best the requirements of particular applications, and the estimation of the applied forces to the sample.

Fig. 4 shows the martensitic material behaviour of the specimen. After a linear elastic increase of forces over prescribed displacement, phase transformation is initialized. This microstructural rearrangement (detwinning) is accompanied by a highly non-linear material reaction. Due to geometric reasons, inhomogeneous bending states are predominant in the specimen which prevents a flat plateau. However, the onset of the transformation process can eas-

ily be identified ($u = 0.014$ mm). The uploading process simulation is also given in a video sequence (link video2). For a more detailed investigation, the distribution of the martensitic configuration is plotted for various load steps. The initial state is given as a homogeneous distribution of the martensite variant. Since the model calculates three variants (each with a transformation strain in the respective Cartesian direction), the initial value is $1/3$. As expected, the focal points of the ellipse transform first, while the rest of the elliptic part of the specimen transforms at larger loads.

Fig. 5 shows the force/displacement curve of the specimen over the loadsteps during the pre-straining and the following heat treatment. This curve is identical to the one presented in Fig. 4 up to a resultant force of zero Newton (load step 265) during the mechanical loading and unloading. After mechanical unloading, temperature is increased linearly with fixed displacements at the left and right hand side of the boundary value problem. While the material transforms temperature-driven from the martensitic composition to the austenite state, the resultant force increases due to the fixed boundary conditions. Small variations of the microstructure induce large forces (load steps 400 and 600). The back transforma-

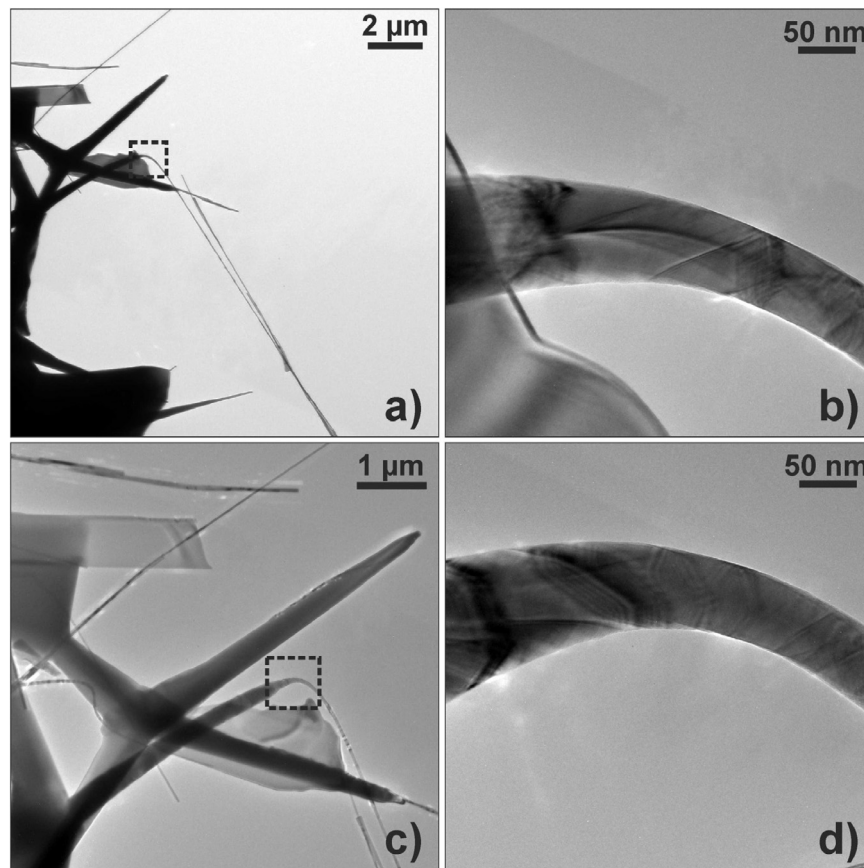


Fig. 8. TEM Images presenting a bent wire as part of the ZnO network at different temperatures: a)+b) 71 °C, c)+d) 90 °C.

tion of very small martensitic zones (load step 1000, red circles) requires a remarkably higher temperature increase as compared to the beginning (load step 400). This effect decreases the slope of the curve. Finally, the force converges since the specimen has completely transformed to austenite.

Due to the geometry, large distortions may be expected during mechanical loading. This would require formulating the model in the context of large deformation. This topic is beyond the scope of the present contribution. We therefore emphasize here that some derivations between experimental and numerical force/displacement relations may be expected which we have to neglect during the further discussion. Details on the implementation of the model into a finite element routine are given in [18].

The numerical simulations allow investigating the distribution of the martensitic variants and thus detect the most loaded zones. Furthermore, the thermo-mechanically coupled structure behaviour can be studied.

3.3. TEM *in situ* experiments

In situ TEM heating experiments show the linearity of the temperature dependence of the gap width for an unloaded as well as for a loaded grid. Starting at room temperature with a gap width of ca. 20 μm for an unloaded grid this width increased initially slowly with 200 nm/K up to the austenite starting temperature at almost 50 °C. From this temperature the underlying function of the grid started and the gap width extended at a rate of 800 nm/K (Fig. 6, square symbols). For a grid loaded with a ZnO network another design was used where the starting gap width was already 120 μm. For this grid an extended linear rate of 2.2 μm/K is given at temperatures above 60 °C due to the modified design (Fig. 6, trian-

gle symbols). The heating rate of the holder was set to 1.5 K/min. For recording images the heating ramp was paused. During this time the increase of gap distance was not proceeding demonstrating high mechanical reliability of the Functional Grid. Experiments with several designs show that the velocity of gap broadening is strongly dependent on the grid design.

Fig. 7 and a video sequence (link video1) illustrate the influence of the straining on the 3-dimensional ZnO network using the Functional Grid. During the experiment the gap width is increasing from initially 120 μm to more than 180 μm. The individual building blocks of the ZnO network are interconnected through entangled wires and tetrapods. These links are stretched during the increase of gap distance. As a result crystalline wires which are fixed on static parts of the network are progressively bent reaching angles beyond 90° with increasing temperature (cf. Fig. 8). Tetrapods as integral part are connected via two of its arms to the rest of the network. Under straining the tetrapods are observed to rotate, as shown in the detail enlargements in Fig. 7e–h).

4. Discussion

The results of the micro tensile tests and the finite elements simulations are similar within certain limits. The shape of the curves corresponds and the remaining displacement at a force of 0 N is 0.2 mm. This correlation argues for the assumption that the simulated forces for the *in situ* heating experiment inside the TEM (up to 0.6 N) are also reliable. This maximum applicable force is large enough to treat samples with a small cross-sectional area like TEM samples which has to be electron transparent. The agreement between the tensile tests and the simulations is a prerequisite for the prediction of suitable grid designs.

The exemplification of the Functional Grids with 3D ZnO network samples shows the observability of changes in the morphology during the *in situ* straining experiment. Until now we have confined on the observation of morphology changes but due to the possibility to controllably terminate and to resume again the heating process it should also be possible to perform electron diffraction on proper samples sequentially *in situ*.

Our future work should exceed the present proof of principle. Besides network samples also thin film samples, e.g. polymer / nanoparticle composites, are intended to be strained with the Functional Grids, although the mounting and required thinning via focussed ion beam milling is yet very sophisticated.

Other mechanical modes like compression or torsion should be accessible with modified grid designs. It is conceivable to design grids which have more than one spring so one can cycle proper samples with these Functional Grids. Even the allocation of electrical contacts seems feasible to monitor the alteration of electrical properties during sample straining.

5. Conclusion

In this work we have shown the possibility to produce Functional Grids out of NiTi shape memory thin films for *in situ* straining of samples in the TEM using customary heating holders. The functionality was demonstrated at 3D ZnO networks where single wires were bent and tetrapods as part of the network were distorted.

Finite elements methods have shown that the elliptic spring is loaded most and all mechanically induced phase transformations are confined. Furthermore, numerical simulations have revealed that the increase of temperature results in a remarkable large force which once again shows the potential of shape memory alloys for actuator systems. The values at the pre-straining process were verified with a micro tensile testing device.

Acknowledgements

This work was funded by the German Research Foundation (DFG) as part of the Collaborative Research Center 1261–Magnetolectric sensors from composite materials to biomagnetic diagnostics (SFB 1261). The authors want to thank Christin Szillus, Matthias Frank, Niko Carstens and Christiane Zamponi for sample preparation. We thank Dustin R. Jantos for the creation of the finite element mesh.

Supplementary materials

Supplementary material associated with this article can be found, in the online version, at [doi:10.1016/j.ultramic.2017.06.003](https://doi.org/10.1016/j.ultramic.2017.06.003).

References

- [1] F.M. Ross, *In situ* transmission electron microscopy, in: P.W. Hawkes, J.C.H. Spence (Eds.), *Science of Microscopy*, Springer, New York, 2007, pp. 445–534.
- [2] U. Schürmann, M. Winkler, J.D. König, X. Liu, V. Duppel, W. Bensch, H. Böttner, L. Kienle, *In Situ TEM investigations on thermoelectric Bi₂Te₃/Sb₂Te₃ multilayers*, *Adv. Eng. Mater.* 14 (3) (2012) 139–143.
- [3] A. Asthana, K. Momeni, A. Prasad, Y.K. Yap, R.S. Yassar, *In situ* probing of electromechanical properties of an individual ZnO nanobelt, *Appl. Phys. Lett.* 95 (17) (2009) 172106.
- [4] S. Yang, L. Wang, X. Tian, Z. Xu, W. Wang, X. Bai, E. Wang, *The piezotronic effect of zinc oxide nanowires studied by in situ TEM*, *Adv. Mater.* 24 (34) (2012) 4676–4682.
- [5] T. Yokota, M. Murayama, J.M. Howe, *In situ* transmission-electron-microscopy investigation of melting in submicron Al-Si alloy particles under electron-beam irradiation, *Phys. Rev. Lett.* 91 (26) (2003) 265504.
- [6] M. Deng, V. Hrkac, U. Schürmann, B. Erkartal, N. Wolff, K. Gerwien, B. Hesseler, F. Beiroth, W. Bensch, V. Duppel, L. Kienle, *Nanocomposite CdSe/Cr₂Se₃: synthesis, characterization, and in situ transformation study*, *Z. Anorg. Allg. Chem.* 641 (2) (2015) 214–220.
- [7] D.C. Bufford, D. Stauffer, W.M. Mook, S.A.S. Asif, B.L. Boyce, K. Hattar, *Combining orientation mapping and in situ TEM to investigate high-cycle fatigue and failure*, *Microsc. Microanal.* 22 (S3) (2016) 1736–1737.
- [8] E. Izadi, A. Darbal, P. Peralta, J. Rajagopalan, *In situ TEM Straining of ultrafine-grained aluminum films of different textures using automated crystal orientation mapping*, *Microsc. Microanal.* 22 (S3) (2016) 1950–1951.
- [9] K. Otsuka, X. Ren, *Physical metallurgy of Ti–Ni-based shape memory alloys*, *Prog. Mater. Sci.* 50 (5) (2005) 511–678.
- [10] J. Frenzel, A. Wiczorek, I. Opahle, B. Maaß, R. Drautz, G. Eggeler, *On the effect of alloy composition on martensite start temperatures and latent heats in Ni–Ti-based shape memory alloys*, *Acta Mater.* 90 (2015) 213–231.
- [11] C. Chluba, W. Ge, R.L. de Miranda, J. Strobel, L. Kienle, E. Quandt, M. Wuttig, *Ultralow-fatigue shape memory alloy films*, *Science* 348 (6238) (2015) 1004–1007.
- [12] Y.K. Mishra, S. Kaps, A. Schuchardt, I. Paulowicz, X. Jin, D. Gedamu, S. Freitag, M. Claus, S. Wille, A. Kovalev, S.N. Gorb, R. Adelung, *Fabrication of macroscopically flexible and highly porous 3d semiconductor networks from interpenetrating nanostructures by a simple flame transport approach*, *Part. Part. Syst. Charact.* 30 (9) (2013) 775–783.
- [13] Y.K. Mishra, G. Modi, V. Cretu, V. Postica, O. Lupan, T. Reimer, I. Paulowicz, V. Hrkac, W. Benecke, L. Kienle, R. Adelung, *Direct growth of freestanding ZnO tetrapod networks for multifunctional applications in photocatalysis, UV photodetection, and gas sensing*, *ACS Appl. Mater. Interfaces* 7 (26) (2015) 14303–14316.
- [14] R. Lima de Miranda, C. Zamponi, E. Quandt, *Micropatterned freestanding superelastic TiNi films*, *Adv. Eng. Mater.* 15 (1–2) (2013) 66–69.
- [15] E. Quandt, C. Zamponi, R. Lima de Miranda, *Method for producing a medical functional element comprising a selfsupporting lattice structure*, US8758636 B2 (2014).
- [16] P. Junker, S. Jaeger, O. Kastner, G. Eggeler, K. Hackl, *Variational prediction of the mechanical behavior of shape memory alloys based on thermal experiments*, *J. Mech. Phys. Solids* 80 (2015) 86–102.
- [17] P. Junker, *An accurate, fast and stable material model for shape memory alloys*, *Smart Mater. Struct.* 23 (11) (2014) 115010.
- [18] P. Junker, K. Hackl, *Calibration and finite element implementation of an energy-based material model for shape memory alloys*, *Shape Mem. Superelasticity* (2016) 1–7.